EVS30 Symposium
Stuttgart, Germany, October 9 - 11, 2017

Energy-Efficient Cruise Control Using Optimal Control for a Hybrid Electric Vehicle

Daliang Shen[1], Dominik Karbowski[1], Jongryeol Jeong[1], Namdoo Kim[1], Aymeric Rousseau[1]

[1]*Argonne National Laboratory, 9700 South Cass Avenue, Argonne, IL 60439, USA,*

E-Mail: dshen@anl.gov; Tel.: +1 630 252 4254

Summary

Increasing connectivity in passenger vehicles provides for a large amount of look-ahead information about driving conditions. An intelligent control algorithm is presented that takes advantage of this information to obtain the operation strategy for the powertrain of a parallel hybrid electric vehicle, in an uncongested highway cruising situation. In order to guarantee sufficient computational efficiency to meet future online requirements, the algorithm is based on Pontryagin's Minimum Principle. The whole driving/operation strategy is composed of a series of solutions to the optimal control sub-problem for each separate route segment. The control sequence computed offline is then evaluated in Autonomie. The simulation result shows 6% fuel savings compared to a baseline rule-based controller with no speed optimization.

Keywords: automated driving, optimization, powertrain, HEV

1 Introduction

Vehicles are now increasingly connected to each other and to the infrastructure, which provides the vehicle controller with abundant information about future driving conditions. Connected digital maps on advanced navigation systems are able to give information such as speed limits, the average speed of traffic, and road geometry and topography. Such information allows the vehicle controller to adjust the powertrain operation and the vehicle speed in automated driving to prepare for upcoming events, and thus achieve a higher overall efficiency, compared to reacting directly to the current situation.

Several interesting studies in the literature regarding speed optimization to improve fuel economy for on-road vehicles are worth mentioning. Generally, an optimal control problem is formulated with the objective of minimizing fuel/energy consumption over a given distance or travel time, subject to different constraints, due to traffic laws as well as the physical limitations of components and passengers. To solve such a problem, Dynamic Programming (DP) is an often utilized technique [1, 2, 3]. Despite its capability to provide a global optimal solution, DP is also known for its heavy computational burden.

In pursuit of reducing the computational cost, we turned to an alternative approach, Pontryagin's Minimum Principle (PMP). Using proper approximations, such as in [4] with piecewise affine consumption models, and in [5] by neglecting aerodynamic resistance for urban driving scenarios, PMP leads to analytical solutions. A semi-analytical approach for heavy engine-driven trucks is proposed in [6] based on a detailed vehicle model. The approach employed by [7, 8] relies on the optimality condition of the constant Hamiltonian to find the instantaneous optimal control variable, depending on a pair of parameters.

Our work follows the general concept of [7, 8] and extends its application to hybrid electric powertrains. This paper provides a method for determining preliminary values for the unknown parameters based on a steady-state assumption. Furthermore, the process to construct a comprehensive speed trajectory out of segments is introduced in this paper, with attention paid to the intrinsic consistency conditions.

2 System Modeling

We used a parallel hybrid electric vehicle (HEV) to conduct a study of speed optimization. The investigated HEV is equipped with a pre-transmission parallel hybrid powertrain, as illustrated in Fig. 1.

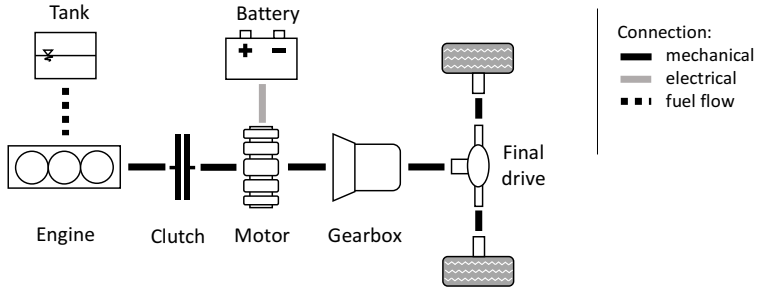

Figure 1: Powertrain of the investigated parallel HEV

2.1 Vehicle Model

A vehicle running on the road overcomes different resistance forces with a traction force F_t. Its longitudinal dynamics fulfills Newton's Second Law of Motion [9]:

$$m\dot{v} = F_\mathrm{t} - F_\mathrm{b} - (c_0 + c_1 v + c_2 v^2) - c_\mathrm{mg} \sin\alpha. \tag{1}$$

Here, m denotes the equivalent mass that consists of the inertia of the rotating parts and the total vehicle mass; v is the vehicle speed. The total braking force is denoted by F_b. The trinomial with coefficients c_0, c_1, and c_2 between the parentheses makes up the resistance forces such as rolling friction and aerodynamic drag. The term with the coefficient of vehicle weight c_mg and the road slope α represents the uphill driving force.

The velocity kinematics describes the vehicle speed as the derivative of the traveled distance s,

$$\dot{s} = v. \tag{2}$$

The traction force F_t is delivered through the drivetrain by the engine and the electric motor (see Fig. 1),

$$F_\mathrm{t} = (T_\mathrm{e} + T_\mathrm{m}) \cdot \gamma \eta^{\mathrm{sign}(T_\mathrm{e}+T_\mathrm{m})}. \tag{3}$$

The torques produced by the engine and the electric motor are denoted with T_e and T_m respectively. The overall transmission ratio γ comprises all the reduction ratios of the gearbox, the final drive, and the wheel. The efficiency η takes account of losses along the drivetrain. Note that the values of m, γ, and η depend on the engaged gear.

Torques T_e and T_m must satisfy the constraints imposed by the physical limits of the engine and the electric components including the motor and the battery,

$$T_\mathrm{e} \in [T_\mathrm{e}^\mathrm{min}(\omega), T_\mathrm{e}^\mathrm{max}(\omega)], \quad T_\mathrm{m} \in [T_\mathrm{m}^\mathrm{min}(\omega), T_\mathrm{m}^\mathrm{max}(\omega)], \tag{4}$$

where the limits vary depending on rotation speed ω. The engine and the motor share the same rotation speed ω, since they are immediately linked when the clutch is closed (see Fig. 1).

2.2 Energy Consumption Model

With the objective of optimizing fuel efficiency, it is necessary to model fuel consumption as a function of engine operating points. In practice, a fuel consumption map is provided on a contour graph of output torque versus rotation speed. Saerens has discussed several models using polynomial equations of different degrees [8]. To capture the hyperbolic behavior of the specific fuel consumption (fuel rate divided by output mechanical power) with respect to both torque and speed, a polynomial approximation of the following expression was chosen to model fuel consumption,

$$P_{\mathrm{f}}(\omega, T_{\mathrm{e}}) = c_{\mathrm{f}01}T_{\mathrm{e}} + c_{\mathrm{f}02}T_{\mathrm{e}}^2 + c_{\mathrm{f}10}\omega + c_{\mathrm{f}11}T_{\mathrm{e}}\omega + c_{\mathrm{f}12}T_{\mathrm{e}}^2\omega + c_{\mathrm{f}20}\omega^2 + c_{\mathrm{f}21}T_{\mathrm{e}}\omega^2, \tag{5}$$

where coefficients $c_{\mathrm{f}\{0,1,2\}\{0,1,2\}}$ are estimated using linear squares surface fitting. Fuel power P_{f} is the chemical energy in fuel set free per unit second, which is proportional to the fuel mass flow rate.

The energy consumption on the electric path must be considered as well. Thereby, the components associated with energy conversion from electric to mechanic form (i.e., the battery and the motor) can be considered as one unit. Thus, the internal battery power P_{bat} that is the negated derivative of the stored energy E_{bat} in the battery, (i.e., $P_{\mathrm{bat}} = -\dot{E}_{\mathrm{bat}}$,) is considered for modeling. P_{bat} can be expressed with polynomial approximation as with fuel consumption, taking into account power losses on both the battery inner resistance and the motor,

$$P_{\mathrm{bat}}(\omega, T_{\mathrm{m}}) = c_{\mathrm{b}01}T_{\mathrm{m}} + c_{\mathrm{b}10}\omega + c_{\mathrm{b}11}T_{\mathrm{m}}\omega + c_{\mathrm{b}12}T_{\mathrm{m}}^2\omega + c_{\mathrm{b}21}T_{\mathrm{m}}\omega^2 + c_{\mathrm{b}22}T_{\mathrm{m}}^2\omega^2, \tag{6}$$

with coefficients $c_{\mathrm{b}\{0,1,2\}\{0,1,2\}}$.

3 Optimal Control on a Road Segment

3.1 Optimal Control Formulation

In reference to the system dynamics (1) and (2) and given the initial conditions and final conditions for state variables v and s,

$$v(0) = v_0, \qquad s(0) = s_0, \tag{7}$$

$$v(t_{\mathrm{f}}) = v_{\mathrm{f}}, \qquad s(t_{\mathrm{f}}) = s_{\mathrm{f}}, \tag{8}$$

we aim to find the time sequence of the optimal control that minimizes the cost function subject to control constraints (4),

$$J = \int_0^{t_{\mathrm{f}}} P_{\mathrm{f}}(\omega, T_{\mathrm{e}}) + \lambda_{\mathrm{E}} P_{\mathrm{bat}}(\omega, T_{\mathrm{m}})\,\mathrm{d}t, \tag{9}$$

where a parameter λ_{E} is introduced to weight the energy usage on the fuel and battery paths. Usage of the battery energy is directly related to λ_{E}. Within the context of the investigated problem, the control vector consists of the engine and motor torques and the braking force, $\boldsymbol{u} = [T_{\mathrm{e}}, T_{\mathrm{m}}, F_{\mathrm{b}}]^\top$. Rotation speed ω is directly related to vehicle speed, $\omega = \gamma v$.

According to the optimal control theory [10], the Hamiltonian for the problem is

$$\begin{aligned} H_i(\boldsymbol{x}, \boldsymbol{\lambda}, \boldsymbol{u}) = \;& P_{\mathrm{f}} \cdot k_i + \lambda_{\mathrm{E}} P_{\mathrm{bat}} + \lambda_{\mathrm{v}}\dot{v} + \lambda_{\mathrm{s}}\dot{s} \\ =\; & P_{\mathrm{f}}(\gamma_i v, T_{\mathrm{e}}) \cdot k_i + \lambda_{\mathrm{E}} P_{\mathrm{bat}}(\gamma_i v, T_{\mathrm{m}}) \\ & + \lambda_{\mathrm{v}} m_i^{-1} \left((T_{\mathrm{e}} \cdot k_i + T_{\mathrm{m}}) \cdot \gamma_i \eta_i^{\mathrm{sign}(T_{\mathrm{e}}+T_{\mathrm{m}})} - F_{\mathrm{b}} - (c_0 + c_1 v + c_2 v^2) - c_{\mathrm{mg}} \sin\alpha(s) \right) \\ & + \lambda_{\mathrm{s}} v. \end{aligned} \tag{10}$$

Hereby, the co-state vector $\boldsymbol{\lambda}$ contains two elements corresponding to states $\boldsymbol{x} = [v, s]^\top$, respectively, $\boldsymbol{\lambda} = [\lambda_\mathrm{v}, \lambda_\mathrm{s}]^\top$. The subscript $\cdot_i$ denotes the powertrain mode, corresponding to the discrete state within the context of hybrid optimal control problems [11]. In this problem, $i \in \mathcal{I} = \{1,2,\dots,n_\mathrm{i}\}$, where the set $\mathcal{I}$ results from the combination of gears and clutch opening/closing, and thus n_i equals two times the number of gears. Depending on i, $k_i \in \{0,1\}$, corresponding to an opened or closed clutch.

3.2 Solution Using PMP Conditions

Without loss of generality, in the following, the discrete state i is first not explicitly denoted.

PMP indicates the optimal control should satisfy

$$\boldsymbol{u}^* = \arg\min_{\boldsymbol{u}} H(\boldsymbol{x}, \boldsymbol{\lambda}, \boldsymbol{u}). \tag{11}$$

It leads to the equation for the locally (unbounded) optimal engine torque T_e^o when it stays within the feasible region (4) and $k_i = 1$,

$$\frac{\partial H}{\partial T_\mathrm{e}}[T_\mathrm{e}^o] = \frac{\partial P_\mathrm{f}}{\partial T_\mathrm{e}} + \lambda_\mathrm{v} m^{-1} \gamma \eta^{\mathrm{sign}(T_\mathrm{e}+T_\mathrm{m})} = 0; \tag{12}$$

in the case of $k_i = 0$, the impact of engine torque is completely eliminated from the Hamiltonian, and we assume the engine is turned off. The same process applies to the locally (unbounded) optimal motor torque T_m^o, when T_m^o fulfills (4),

$$\frac{\partial H}{\partial T_\mathrm{m}}[T_\mathrm{m}^o] = \lambda_\mathrm{E} \frac{\partial P_\mathrm{bat}}{\partial T_\mathrm{m}} + \lambda_\mathrm{v} m^{-1} \gamma \eta^{\mathrm{sign}(T_\mathrm{e}+T_\mathrm{m})} = 0. \tag{13}$$

Since P_f and P_bat adopt quadratic models, $\frac{\partial P_\mathrm{f}}{\partial T_\mathrm{e}}$ and $\frac{\partial P_\mathrm{bat}}{\partial T_\mathrm{m}}$ are linear. Thus, combining (12) and (13) results in an affine relation between T_e^o and T_m^o, rewritten as

$$T_\mathrm{m}^o = \sigma_1 T_\mathrm{e}^o + \sigma_0, \tag{14}$$

where coefficients σ_1 and σ_0 are dependent on v and λ_E.

This paper follows the method initiated in [7]. It is based upon the fact that the Hamiltonian does not explicitly depend on time, which makes its value constant,

$$H(t) = \mathfrak{H} \neq 0, \qquad \forall\ t \in [0, t_\mathrm{f}]. \tag{15}$$

Furthermore, PMP links the dynamics of the co-states with the Hamiltonian:

$$\dot{\lambda}_\mathrm{s} = -\frac{\partial H}{\partial s} = \lambda_\mathrm{v} m^{-1} c_\mathrm{mg} \cos\alpha(s) \cdot \frac{\partial \alpha}{\partial s}. \tag{16}$$

We assume road slopes are piecewise constant, which leads to λ_s being piecewise constant as well.

Inserting (12), (13) and (15) into (10) yields quadratic equations for T_m^o and T_e^o in terms of variable v and parameters λ_s, λ_E, and $\mathfrak{H}$.

Now considering the control constraints, the optimal control for the engine torque is

$$T_\mathrm{e}^* = \begin{cases} T_\mathrm{e}^{\max} & \text{if } T_\mathrm{e}^o \geq T_\mathrm{e}^{\max} \\ T_\mathrm{e}^o(v, s|\lambda_\mathrm{E}, \mathfrak{H}, \lambda_\mathrm{s}) & \text{if } T_\mathrm{e}^{\min} < T_\mathrm{e}^o < T_\mathrm{m}^{\max}, \\ T_\mathrm{e}^{\min} & \text{if } T_\mathrm{e}^o \leq T_\mathrm{e}^{\min} \end{cases} \text{for } k_i = 1; \quad T_\mathrm{e}^* = 0, \text{ for } k_i = 0. \tag{17}$$

As for the optimal motor torque, applying the control constraints, the optimal control for the engine torque is derived as

$$T_{\mathrm{m}}^{*} = \begin{cases} T_{\mathrm{m}}^{\max} & \text{if } T_{\mathrm{m}}^{o+} \geq T_{\mathrm{m}}^{\max} \\ T_{\mathrm{m}}^{o}(v, s|\lambda_{\mathrm{E}}, \mathfrak{H}, \lambda_{\mathrm{s}}) & \text{if } T_{\mathrm{m}}^{\min} < T_{\mathrm{m}}^{o-} < T_{\mathrm{m}}^{\max} \\ T_{\mathrm{m}}^{\min} & \text{if } T_{\mathrm{m}}^{o-} \leq T_{\mathrm{m}}^{\min} \end{cases}. \tag{18}$$

By substituting (15) in (10), λ_{v} is evaluated,

$$\lambda_{\mathrm{v}} = -m \cdot \frac{k_i P_{\mathrm{f}}(\gamma v, T_{\mathrm{e}}) + \lambda_{\mathrm{E}} P_{\mathrm{bat}}(\gamma v, T_{\mathrm{m}}) + \lambda_{\mathrm{s}} v - \mathfrak{H}}{(k_i T_{\mathrm{e}}^{*} + T_{\mathrm{m}}^{*}) \cdot \gamma \eta^{\mathrm{sign}(k_i T_{\mathrm{e}}^{*} + T_{\mathrm{m}}^{*})} - F_{\mathrm{b}} - (c_0 + c_1 v + c_2 v^2) - c_{\mathrm{mg}} \sin\alpha} \ . \tag{19}$$

Applying (11), the last control variable F_{b} is determined, as a switching function of λ_{v},

$$F_{\mathrm{b}}^{*} = \begin{cases} 0 & \text{if } \lambda_{\mathrm{v}} \leq 0 \\ F_{\mathrm{b}}^{\max} & \text{if } \lambda_{\mathrm{v}} > 0 \end{cases} \tag{20}$$

where $F_{\mathrm{b}}^{\max}$ is the upper limit of braking force.

So far, all the control variables (for each i) have been derived, and they are ultimately dependent only on v. The last step is to choose the proper discrete state i, since the switching of i in our problem is actively controlled. According to the hybrid optimal control theory [11], the optimal discrete state should minimize the Hamiltonian. In other words, the discrete state i, with the correspondent λ_{v} from (19) that makes its correspondent H_i minimum among $i \in \mathcal{I}$, is considered optimal. Once i is determined, the correspondent control is selected as the final solution.

In summary, the necessary conditions lead to a closed-form expression $\boldsymbol{u}$ to calculate the optimal controls and the discrete state, $[\boldsymbol{u}^{*}, i^{*}]^{\top} = \boldsymbol{u}(\boldsymbol{x}|\lambda_{\mathrm{E}}, \mathfrak{H}, \lambda_{\mathrm{s}})$. Inserting the locally optimal control signals $[\boldsymbol{u}^{*}, i^{*}]^{\top}$ to the system dynamics (1) and (2) results in formation of state trajectories solely depending on parameters λ_{E}, $\mathfrak{H}$, and λ_{s}.

3.3 Estimation of Parameters

With a given v at an arbitrary time t, the optimal control can be found, as shown in Section 3.2. Thereby, parameters λ_{E}, $\mathfrak{H}$, and λ_{s} are still unknown and have to be determined. As shown in the literature [12, 4, 2], if a route segment with a constant slope is long enough, the vehicle will reach a steady-state speed v_{ss} at the middle stage along an optimized speed trajectory. This behavior can be taken advantage of in order to estimate the unknown parameters.

A meaningful variable to use in the estimation process is the steady-state torque T_{ss} on the input side of the gearbox that maintains the vehicle moving at given constant speed v and slope α:

$$T_{\mathrm{ss}}(v|\alpha) = \big((c_0 + c_1 v + c_2 v^2) + c_{\mathrm{mg}} \sin\alpha\big) \cdot \gamma^{-1} \eta^{-\mathrm{sign}\left((c_0 + c_1 v + c_2 v^2) + c_{\mathrm{mg}} \sin\alpha\right)}. \tag{21}$$

We suppose the driver has given a preferred cruising speed v_{set} for the trip section where the cruise control is activated, and for the purpose of parameter estimation, we also assume that the vehicle runs on a level road most of the time. At that operating point ($v = v_{\mathrm{set}},\ \alpha = 0$), we can guess a value for the equivalence factor λ_{E} by assuming equivalency between the engine-only and pure electric modes in terms of energy cost:

$$P_{\mathrm{f}}(\gamma v_{\mathrm{set}}, T_{\mathrm{ss}}(v_{\mathrm{set}}|\alpha = 0)) = \lambda_{\mathrm{E}} P_{\mathrm{bat}}\big(\gamma v_{\mathrm{set}}, T_{\mathrm{ss}}(v_{\mathrm{set}}|\alpha = 0)\big). \tag{22}$$

Next, parameter $\mathfrak{H}$ is to be determined. The method initiated by [8, 7] for conventional engine-driven cars still applies here. In a steady state with $\alpha = 0$, λ_{s} can be calculated using (10), given the aforementioned equivalency and $\dot{v} = 0$,

$$-\lambda_{\mathrm{s}}(v) = v^{-1} \cdot (P_{\mathrm{f}}(\gamma v, T_{\mathrm{ss}}(v|\alpha = 0)) - \mathfrak{H}). \tag{23}$$

$-\lambda_{\mathrm{s}}$ can be interpreted as a measure for a weighted fuel consumption considering the travel time at a steady-state speed v_{ss}. The chosen $\mathfrak{H}$ should satisfy the condition that $-\lambda_{\mathrm{s}}$ reaches its minimum exactly at target speed $v = v^*_{\mathrm{ss}} = v_{\mathrm{set}}$ (see [8]). In a practical sense, this $\mathfrak{H}$ serves as a general parameter balancing fuel economy and travel time.

3.3.1 Slope changes

If the slope changes (i.e., $\alpha \neq 0$), so should λ_{s} and v^*_{ss}. For $\alpha \neq 0$, the assumed equivalency (22) is no more valid. Therefore, $-\lambda_{\mathrm{s}}(v)$ must account for the fact $T_{\mathrm{ss}} = T_{\mathrm{e,ss}} + T_{\mathrm{m,ss}}$,

$$-\lambda_{\mathrm{s}}(v) = v^{-1} \cdot (P_{\mathrm{f}}(\gamma v, T_{\mathrm{e,ss}}(v|\alpha, \lambda_{\mathrm{E}})) + \lambda_{\mathrm{E}} P_{\mathrm{bat}}(\gamma v, T_{\mathrm{m,ss}}(v|\alpha, \lambda_{\mathrm{E}})) - \mathfrak{H}). \tag{24}$$

The steady-state torques on the engine and the motor, $T_{\mathrm{e,ss}}$ and $T_{\mathrm{m,ss}}$, are determined by (14)(17)(18). With λ_{E} and $\mathfrak{H}$ unchanged, we are able to find a new $v^*_{\mathrm{ss}} = v^o_{\mathrm{ss}}$ that makes $-\lambda_{\mathrm{s}}(v)$ reach its minimum at v^o_{ss}.

3.3.2 Speed limits

If there are speed limits in the route segment, v^*_{ss} must be subject to those limits. Let $v_{\max}$ and $v_{\min}$ denote the upper and lower speed limits. It yields a new target steady-state speed for this segment,

$$v^*_{\mathrm{ss}} = \min\{v_{\max}, \max\{v_{\min}, v^o_{\mathrm{ss}}\}\}. \tag{25}$$

Parameter λ_{s} is easy to acquire using (23), given that $\mathfrak{H}$ and $v_{\mathrm{ss}} = v^*_{\mathrm{ss}}$ are already defined.

In summary, parameters λ_{E} and $\mathfrak{H}$ are constant for the whole travel mission, while λ_{s} is piecewise constant and changes at segment borders.

3.4 Trajectory Construction

Now that the target steady-state speed v^*_{ss} for each segment has been defined, the only remaining question is how the optimal speed behaves at links between segments.

If the slope grade does not change, speed change is then initiated by the change of speed limits. Speed is either "released" from a limit in the previous segment or "grasped" by a limit in the next segment. Fig. 2 displays the first case at the first segment border. The choice of the speed at the segment border v^*_{x} is subject only to speed limits,

$$v^*_{\mathrm{x}|j} = \min\big\{v_{\max|j-1},\, \max\big\{v_{\min|j-1}, v^*_{\mathrm{ss}|j}\big\}\big\} \quad \text{or} \quad \min\big\{v_{\max|j},\, \max\big\{v_{\min|j}, v^*_{\mathrm{ss}|j-1}\big\}\big\}. \tag{26}$$

Suffixes $\cdot_{\cdot|\{j,j-1\}}$ denote the association with the segment. In most cases, roots yielded by (26) should be equal. The roots are not equal only when the feasible regions for the speed of the segments do not intersect. In that case, the higher of the lower speed limits should be ignored and a unique v^*_{x} acquired, as lower limits are generally not strictly defined by traffic laws.

If the slope changes, the speed trajectory is generally away from the boundaries at both sides of the segment border. The necessary condition that λ_{v} must be maintained continuously mandates a specific value for v^*_{x} which equalizes λ_{v} of (19) before and after the slope change – this is solved numerically.

The optimal speed at segment borders v^*_{x} is then selected as the end and start speeds of the previous and following segments, respectively, $v_{\mathrm{f}|j-1}$ and $v_{0|j}$.

Thus far, for each route segment *where the upper and lower speed limits as well as the slope grade keep constant*, a two-point boundary value problem has been built. Using the optimal solution for controls (17), (18), and (20), and λ_{v} with (19) for decision of the powertrain mode i inserted in the system dynamics (1)

and (2), *sub-arcs* of optimal vehicle speed, starting from $v_{0|j}$ and $s_{0|j}$, and ending at $v_{\mathrm{f}|j}$ and $s_{\mathrm{f}|j}$, result from forward and backward integrations. As displayed in Fig. 3a, depending on the relativity between $v_{0|j}$ and $v^*_{\mathrm{ss}|j}$, three cases exist for the starting sub-arc; $T_\mathrm{e}+T_\mathrm{m}>T_\mathrm{ss}$ (case 1), $T_\mathrm{e}+T_\mathrm{m}=T_\mathrm{ss}$ (case 2), and $T_\mathrm{e}+T_\mathrm{m}<T_\mathrm{ss}$ (case 3). Similarly, as summarized in Fig. 3b, there are three cases for the ending sub-arc; $T_\mathrm{e}+T_\mathrm{m}<T_\mathrm{ss}$ (case a), $T_\mathrm{e}+T_\mathrm{m}=T_\mathrm{ss}$ (case b), and $T_\mathrm{e}+T_\mathrm{m}>T_\mathrm{ss}$ (case c). According to Bellman's principle of optimality, the overall optimal solution from $(v_{0|j}, s_{0|j})$ to $(v_{\mathrm{f}|j}, s_{\mathrm{f}|j})$ consists of the starting and ending sub-arcs that correspond to cases 1, 2, and 3, and a, b, and c, respectively (see Fig. 3). A constant-speed section with $v=v^*_{\mathrm{ss}|j}$ is inserted in between to form the complement, if the route segment is long enough for the vehicle to reach the steady state. Otherwise, the overall speed trajectory of the segment is composed either by intersecting the two sub-arcs (if $v_{0|j}$ and $v_{\mathrm{f}|j}$ both are situated on the same side of $v^*_{\mathrm{ss}|j}$) or a single sub-arc connecting $(v_{0|j}, s_{0|j})$ and $(v_{\mathrm{f}|j}, s_{\mathrm{f}|j})$ (if $v_{0|j}$ and $v_{\mathrm{f}|j}$ are situated on two sides of $v^*_{\mathrm{ss}|j}$).

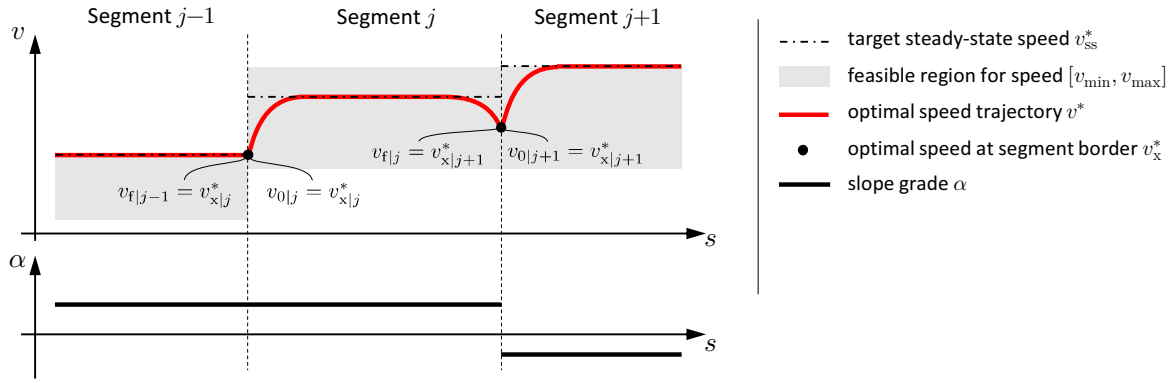

Figure 2: Scheme of optimal speed trajectory on route segments

After the solutions for all the segments of the given route are acquired, they can be connected end to end and the whole speed profile constructed. Meanwhile, since the control sequence shares the same time/distance reference as with the speed trajectory, the complete control policy for the whole route results from editing the speed profile, which can be implemented directly to the vehicle as an open-loop control.

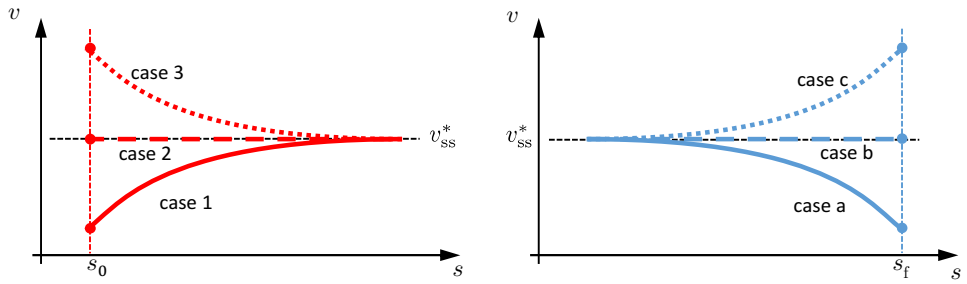

Figure 3: Possible sub-arcs of speed trajectory at the beginning (left) and the end (right) of a route segment

4 Results

4.1 Simulation setup

To evaluate the benefits of the proposed algorithm, we use forward-looking vehicle models developed within Autonomie, a framework for vehicle fuel consumption and performance simulation [13]. We compare the algorithm presented in previous sections with two other control strategies, where the speed is not a direct or indirect degree of freedom, rather a "reference" speed trajectory. For all three strategies, the same vehicle plant models are used.

The baseline strategy is the default rule-based controller for Parallel HEV in Autonomie. The engine is started when the driver power demand is above a certain threshold, and shut down otherwise. When the engine is on, it provides the power for the road load, modulated by a power to regulate the battery state of charge (SoC). In the following, this strategy will be referred to as *baseline*.

The second strategy is an online implementation of PMP developed in [14] adapted to a parallel powertrain. In this strategy, the controller aims at providing the driver requested torque, and computes the optimal torque split using PMP. Multiple simulations are required to find the co-state that results in final SoC close to the initial one. This strategy will be subsequently called *PT-PMP*.

The third strategy is an offline implementation of the energy-efficient cruise-control algorithm. The optimal control policy for $\{T_e, T_m, F_b, i\}$ is first calculated offline using the dynamic model described in (1)(2)(3) and in combination with the optimal control algorithm. The resulting trajectories are then used as control commands for full model simulation, with no feedback loop. This strategy is designated as *DYM+PT-OPT*.

Fig. 4 illustrates the setup of the simulation for the purpose of evaluation.

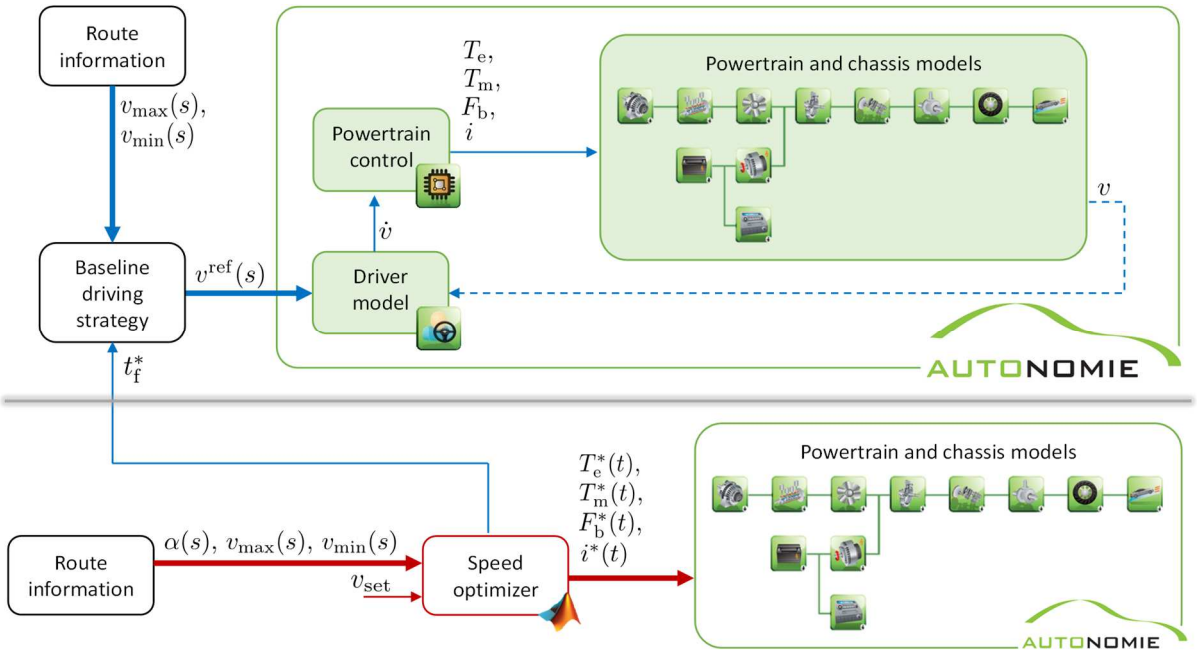

Figure 4: Schematic layout of the simulation setup; baseline and PT-PMP on the top, DYM-PT-OPT on the bottom

4.2 Route and reference speed target

To evaluate the proposed algorithm, we applied it to an example route. The 28-km-long route track has five speed limits and seven slope grades on different locations and of different lengths. The average speed limit is $25.8\ \mathrm{m/s}$ ($93\ \mathrm{km/h}$). The slope ranges from $-0.052\ \mathrm{rad}$ to $0.087\ \mathrm{rad}$, with a total uphill climb of $251\ \mathrm{m}$ and a total downhill descent of $192\ \mathrm{m}$.

To generate the reference, we use a linear decay model [15] that represents average human behavior. We chose parameters for acceleration, $\alpha = 2.68\ \mathrm{m/s^2}$ and $\beta = 0.073\ \mathrm{s^{-1}}$; and for deceleration, $\alpha = -3.23\ \mathrm{m/s^2}$ and $\beta = -0.088\ \mathrm{s^{-1}}$. This models generates realistic transitions between target speed changes for the baseline and PT-PMP strategies. Fig. 5 shows the route as well as the reference speed.

4.3 Optimization Result

By applying the proposed algorithm, the whole route is first divided into 30 segments, according to the road attributes; that is, fulfilling the requirement that each segment has constant speed limit and slope (see Fig. 6).

The desired travel speed v_{set} is set by the driver at $25\ \mathrm{m/s}$. General parameters λ_E and $\mathfrak{H}$ are determined as explained in Section 3.3, $\lambda_E = 2.502$ and $\mathfrak{H} = -5.63 \times 10^4\ \mathrm{W}$. Parameter λ_s varies from segment to

segment, in compliance with different v^*_{ss}, which is illustrated in Fig. 6 with the green dash-dotted line. With v^*_{ss} as the guideline, the algorithm forms the energy-efficient optimal speed profile using the methodology proposed in Section 3.4.

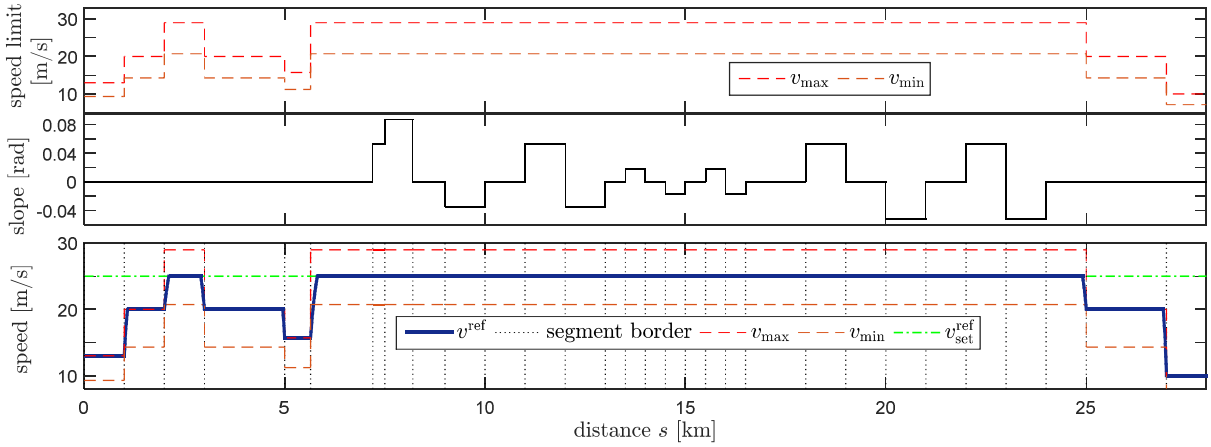

Figure 5: Example route (above) and reference speed profile (below)

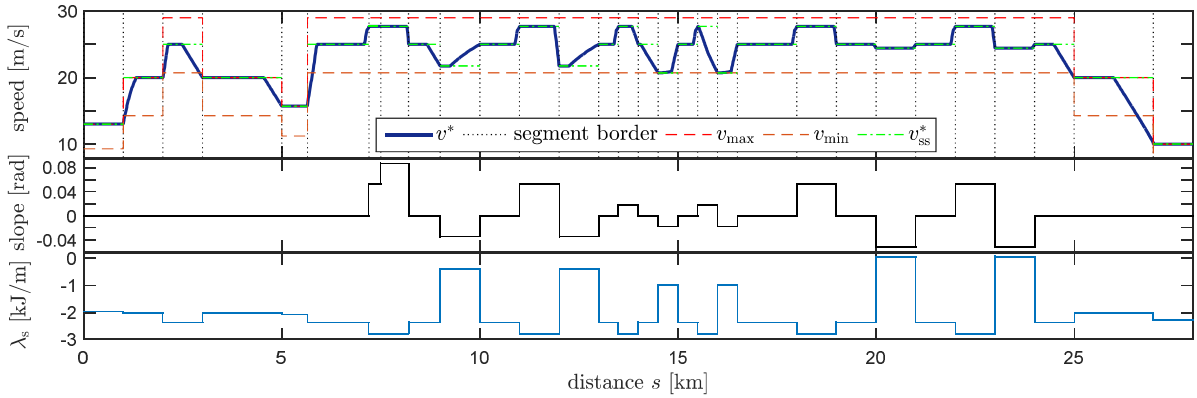

Figure 6: Optimized speed profile for the example track

4.4 Simulation

The simulation result indicated that the initial guess for λ_{E} was too low and that the battery SoC fell below the lower limit. As we changed λ_{E}, so did $\mathfrak{H}$ and the resulting optimal speed profile (see Fig. 7a). Correspondingly, the simulation results regarding the travel time and end SoC fluctuated (see Fig. 7b).

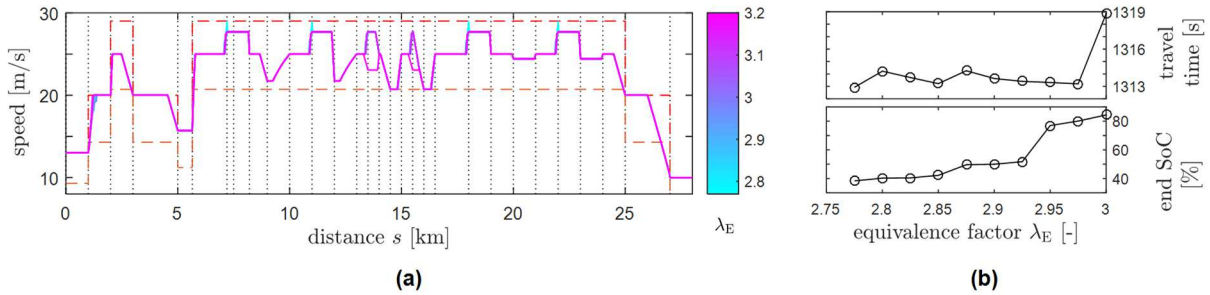

Figure 7: Changes in response to λ_{E}. **(a)** Optimization result of speed **(b)** Simulation result of end SoC and travel time

We selected the optimization results with a final SoC of 51.8% closest to the initial value of 60% corresponding to $\lambda_{\mathrm{E}} = 2.925$ for comparative study (see Fig. 7b). Fig. 8 compares the speed trajectory computed offline by the proposed algorithm and the simulation result of the direcly applied control policy,

showing only slight deviations despite its open-loop-control nature. The set speed $v_{\text{set}}^{\text{ref}} = 24.2\ \text{m/s}$ for the baseline strategy was chosen to match the same travel time t_{f}^{*} as for the optimal profile (see Fig. 5).

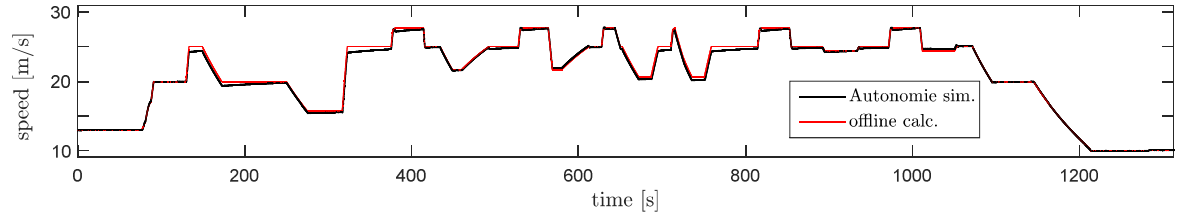

Figure 8: Comparison of speeds of offline calculation and Autonomie simulation result for the second strategy

The comparison of the simulation results using the baseline, PT-PMP, and DYM+PT-OPT is displayed in Fig. 9. The results regarding the SoC trace indicate that DYM+PT-OPT utilized the battery more gently compared to the other two strategies. A closer look at the battery power curves shows that the battery was far less charged in DYM+PT-OP than in the other two. We can infer that DYM+PT-OP leveraged the extra degree of freedom in speed besides the energy reserve in the battery to optimally distribute the propulsion power throughout the travel mission, and avoided charging from the engine. In fact in DYM+PT-OP, 13% of the engine output energy was used towards charging the battery, while this number is 10 points higher in the other two cases (see Table 1).

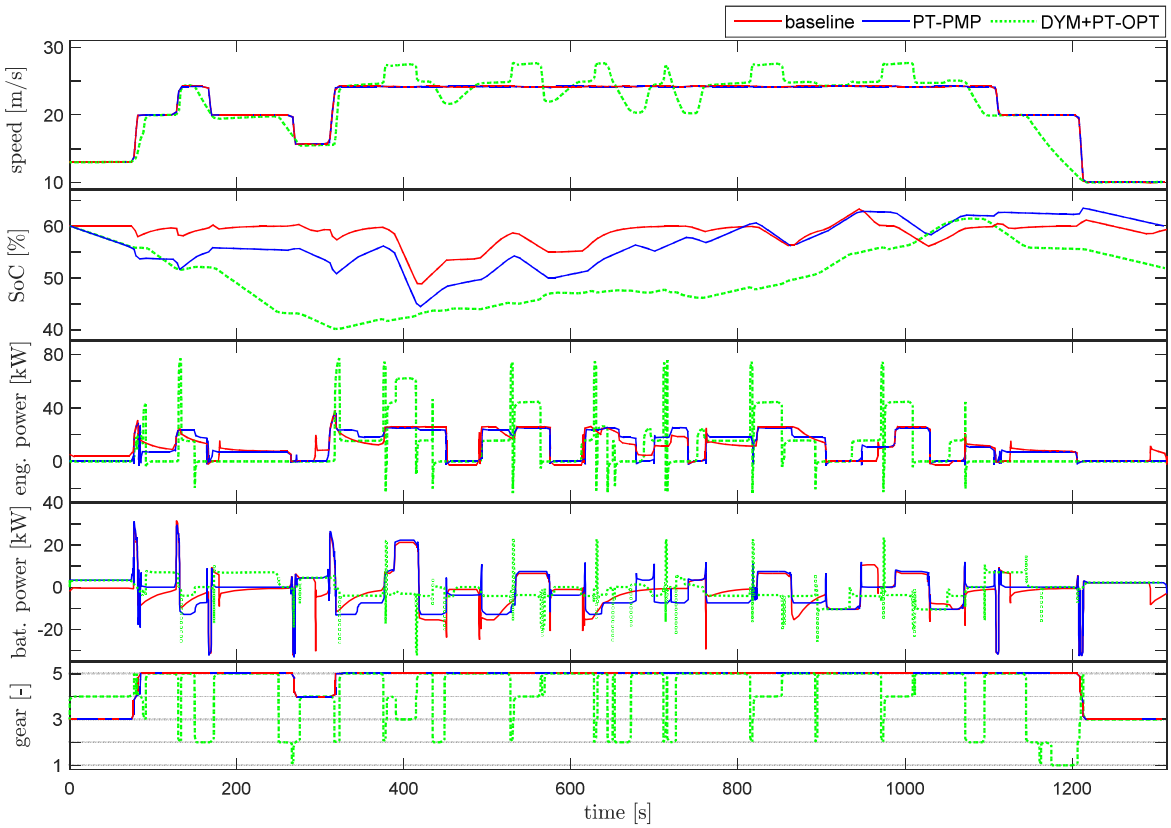

Figure 9: Comparison of simulation results using baseline, PT-PMP, and DYM+PT-OPT

Table 1: Comparative evaluation of simulation results of the three strategies

	avg. speed [m/s]	num. of engine starts [-]	engine-on duration [s]	avg. eng. efficiency [%]	ratio of fuel used for charging [%]	fuel [kg]	end SoC [%]	adj. fuel consumption [L/100 km]	adj. saving [%]
baseline	21.31	7	1068.9	33.11	22.07	1.024	59.29	4.953	-
PT-PMP	21.31	17	870.7	34.31	23.67	1.000	59.88	4.821	2.68
DYM+PT-OPT	21.16	18	507.4	34.42	13.52	0.917	51.75	4.689	6.02

Comparative evaluation in Table 1 confirmed the noticeable saving potential in driving strategy. The fuel saving figure is corrected, thereby taking account of final SoC deviations. Note that the savings were achieved without noticeable decrease in average speed. Even though powertrain operation in PT-PMP had already been optimized by PMP-based optimal control, DYM+PT-OPT was still able to achieve 3.3 percentage points more fuel saving.

5 Conclusion

A PMP-based algorithm has been proposed to generate an energy-efficient speed profile on a given route for a parallel HEV. The algorithm divides the whole travel route into segments and the speed is chosen at each junction relying on intrinsic optimality conditions. Using an analytical solution for control variables derived from PMP conditions, the algorithm arrives at an optimal speed profile by combining the results of each segment. The proposed algorithm was simulated in Autonomie, showing 6% fuel savings compared to a baseline rule-based controller with no speed optimization, and still shows 3.3% savings when the powertrain is optimized (but still without speed optimization).

To better understand the potential real-world performance of the proposed algorithm, future work will include online implementation with close-loop control feedback, as well as taking into account drivability constraints. Furthermore, other road attributes will be taken into account, such as pointwise speed limits due to curvature, as well as mandatory stops due to traffic signs. Finally, full energy-saving potential can only be exploited through explicitly incorporating battery energy management, in terms of stored energy, into the optimal control problem. Accordingly, more investigation is necessary to find a quick way to estimate λ_{E}.

Acknowledgments

This work was supported by the U.S. Department of Energy's Vehicle Technologies Office under the direction of Mr. David Anderson. The submitted manuscript has been created by UChicago Argonne, LLC, Operator of Argonne National Laboratory ("Argonne"). Argonne, a U.S. Department of Energy Office of Science laboratory, is operated under Contract No. DE-AC02-06CH11357. The U.S. Government retains for itself, and others acting on its behalf, a paid-up nonexclusive, irrevocable worldwide license in said article to reproduce, prepare derivative works, distribute copies to the public, and perform publicly and display publicly, by or on behalf of the Government.

References

[1] E. Hellström, M. Ivarsson, J. Åslund and L. Nielsen, *Look-ahead control for heavy trucks to minimize trip time and fuel consumption*, Control Engineering Practice, 17(2009), 245–254.

[2] F. Mensing, "Optimal energy utilization in conventional, electric and hybrid vehicles and its application to eco-driving," Lyon, Ph.D. Thesis, INSA de Lyon, 2013.

[3] T.J. Boehme, F. Held, C. Rollinger, H. Rabba, M. Schultalbers, and B. Lampe, *Application of an optimal control problem to a trip-based energy management for electric vehicles*, SAE Int. J. Alt. Power., 2(2013), 115–126.

[4] T. van Keulen, B. de Jager, D. Foster, and M. Steinbuch, "Velocity trajectory optimization in hybrid electric trucks," in *Proceedings of the 2010 American Contrl Conference*, Baltimore, 2010.

[5] W. Dib, A. Chasse, P. Moulin, A. Sciarretta, and G. Corde, *Optimal energy management for an electric vehicle in eco-driving applications*, Control Engineering Practice, 29(2014), 299–307.

[6] B. Passenberg, P. Kock, and O. Stursberg, "Combined time and fuel optimal driving of trucks based on a hybrid model," in *Proc. 10th European Control Conf.*, Budapest, Hungary, 2009.

[7] A.B. Schwarzkopf, and R.B. Leipnik, *Control of highway vehicles for minimum fuel consumption over varying terrain*, Transportation Research, 11(4)(1977), 279–286.

[8] B. Saerens, "Optimal control based eco-driving: theoretical approach and practical applications," Heverlee, Belgium, Ph.D. Thesis, Katholieke Universiteit Leuven, 2012.

[9] L. Guzzella, and A. Sciarretta, *Vehicle propulsion systems: introduction to modeling and optimization*, Springer, Berlin, 2007.

[10] M. Papageorgiou, M. Leibold, und M. Buss, *Optimierung: statische, dynamische, stochastische Verfahren für die Anwendung*, Springer Vieweg, Berlin, 2012.

[11] M.S. Shaikh, and P.E. Caines, *On the hybrid optimal control problem: theory and algorithms,* IEEE Transactions on Automatic Control*,* 52(9)(2007), 1587–1603.

[12] A. Sciaretta, G. de Nunzio, and L.L. Ojeda*, Optimal ecodriving control: energy-efficient driving of road vehicles as an optimal control problem*, IEEE Control Systems*,* 35(5)(2015), 71–90.

[13] Argonne National Laboratory, "Autonomie - Home." Available at www.autonomie.net.

[14] D. Karbowski, N. Kim, and A. Rousseau, "Route-Based Online Energy Management of a PEHV and Sensitivity to Trip Prediction," in *2014 IEEE Vehicle Power and Propulsion Conference*, 2014.

[15] G. Long, *Acceleration Characteristics of Starting Vehicles*, Transportation Research Record: Journal of the Transportation Research Board*,* 1737(2000), 58–70.

Authors

Daliang Shen received his B.S. and B.E. degrees in Mechatronics from Tongji University, China, and Esslingen University of Applied Science, Germany, respectively, in 2010 in a double graduation program. He received his M.S. in Mechatronics from the Friedrich-Alexander-Universität Erlangen-Nürrnberg, Germany, in 2013. He is now pursuing a Ph.D. from Technische Universität Berlin, Germany. He was involved in scientific research at Technische Universität Kaiserslautern, Germany, in 2013, and Technische Universität Berlin, Germany, from 2014 to 2016. He is currently a visiting scholar at Argonne National Laboratory, Argonne, IL. His current research interests include optimal powertrain control and cruise control for passenger vehicles of various powertrain types.

Dominik Karbowski is the Technical Manager in charge of Intelligent Eco-Mobility at Argonne National Laboratory, leading Argonne's research on intelligent powertrain control, energy-efficient connected and automated vehicles. Dominik has extensive experience in automotive systems modelling and simulation, control theory, energy management, electrified powertrain design and optimization, and stochastic characterization of driving in the real-world. Dominik is a major developer of control and component models as well as processes for Autonomie, Argonne's vehicle simulation tool. Dominik holds a Master of Science in Engineering from Mines ParisTech (France).

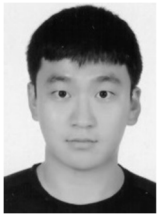

Jongryeol Jeong received his Ph.D. in Mechanical Engineering from Seoul National University in Seoul, Korea, in 2015. The main subject of thesis was optimization of energy management and supervisory control of plug-in hybrid electric vehicle considering thermal aspects of vehicle components. He has been working in Argonne National Laboratory's Vehicle Modeling and Simulation Group as a postdoctoral researcher since 2015. His research includes modeling various vehicle systems and components, validating simulation models, developing vehicle supervisory controls, and optimization of energy management.

Namdoo Kim graduated in 2007 from the University of Sungkyunkwan, Korea, with a master's degree in Mechanical Engineering. After working for Samsung Engineering Co. in the Mechanical Equipment Design Department, he joined Argonne National Laboratory in 2008, where he is now a systems analysis engineer in Vehicle Modeling and Simulation Group. He has extensive experience about research of automotive systems modeling, simulation, control and electrified powertrain design.

Aymeric Rousseau is the manager of the Vehicle Modeling and Simulation Group at Argonne National Laboratory. He received his engineering diploma at the Industrial System Engineering School in La Rochelle, France, in 1997. After working for PSA Peugeot Citroen in the Hybrid Electric Vehicle Research Department, he joined Argonne National Laboratory in 1999, where he is now responsible for the development of Autonomie. He received an R&D 100 Award in 2004 and a 2010 Vehicle Technologies Program Award in 2010. He has authored more than 40 technical papers in the area of advanced vehicle technologies.